JCI The Journal of Clinical Investigation

Targeted hypoxia reduction restores T cell infiltration and sensitizes prostate cancer to immunotherapy

Priyamvada Jayaprakash, … , Tomasz Zal, Michael A. Curran

J Clin Invest. 2018. https://doi.org/10.1172/JCI96268.

Research In-Press Preview **Immunology** **Oncology**

Despite the success of T cell checkpoint blockade against melanoma, many “cold” tumors such as prostate cancer remain unresponsive. We find that hypoxic zones are prevalent across pre-clinical prostate cancer and resist T cell infiltration even in the context of CTLA-4 and PD-1 blockade. We show that the hypoxia-activated prodrug TH-302 reduces or eliminates hypoxia in these tumors. Combination therapy with this hypoxia-prodrug and checkpoint blockade cooperate to cure more than 80% of TRAMP-C2 prostate tumors. Immunofluorescence imaging shows that TH-302 drives an influx of T cells into hypoxic zones, which are then amplified by checkpoint blockade. Further, combination therapy reduces myeloid-derived suppressor cell density by more than 50%, and causes a persistent defect in the capacity of the tumor to replenish the granulocytic subset. Spontaneous prostate tumors in TRAMP transgenic mice, which are completely resistant to checkpoint blockade, show minimal adenocarcinoma tumor burden at 36 weeks of age and no evidence of neuroendocrine tumors. Survival of *Pb-Cre4*, *Ptenpc*$^{-/-}$*Smad4pc*$^{-/-}$ mice with highly aggressive prostate adenocarcinoma is also significantly extended by the combination of hypoxia-prodrug and checkpoint blockade. This combination of hypoxia disruption and T cell checkpoint blockade may render some of the most therapeutically resistant cancers sensitive to immunotherapy.

Title: Targeted hypoxia reduction restores T cell infiltration and sensitizes prostate cancer to immunotherapy

Authors: Priyamvada Jayaprakash[†1], Midan Ai[†1], Arthur Liu[1,2], Pratha Budhani[1], Todd Bartkowiak[1,2], Jie Sheng[1], Casey Ager[1,2], Courtney Nicholas[1], Ashvin R. Jaiswal[1], Yanqiu Sun[1], Krishna Shah[1], Sadhana Balasubramanyam[1], Nan Li[3], Guocan Wang[4], Jing Ning[3], Anna Zal[1], Tomasz Zal[1,2], Michael A. Curran[1,2*].

Affiliations:

1. Department of Immunology, University of Texas MD Anderson Cancer Center, Houston, TX 77054.
2. University of Texas Health Science Center at Houston Graduate School of Biomedical Science, Houston TX, 77054.
3. Department of Biostatistics, University of Texas MD Anderson Cancer Center, Houston, TX 77030
4. Department of Cancer Biology, University of Texas MD Anderson Cancer Center, Houston, TX 77054

† P.J. and M.A. contributed equally to this work.

The authors have declared that no conflict of interest exists.

Running Title: Hypoxia reduction sensitizes prostate cancer to immunotherapy

Keywords: Hypoxia, prostate cancer, immunotherapy, CTLA-4, PD-1

Summary: Reduction of hypoxia with the prodrug TH-302 restores T cell infiltration and sensitizes prostate cancer to checkpoint blockade immunotherapy.

To whom correspondence and requests for materials should be addressed:

Dr. Michael A. Curran
UT MD Anderson Cancer Center
Department of Immunology
1515 Holcombe Blvd.
Unit 901
Houston, TX, 77054, USA
mcurran@mdanderson.org

Abstract:

Despite the success of immune checkpoint blockade against melanoma, many “cold” tumors like prostate cancer remain unresponsive. We found that hypoxic zones were prevalent across pre-clinical prostate cancer and resisted T cell infiltration even in the context of CTLA-4 and PD-1 blockade. We demonstrated that the hypoxia-activated prodrug TH-302 reduces or eliminates hypoxia in these tumors. Combination therapy with this hypoxia-prodrug and checkpoint blockade cooperated to cure more than 80% of tumors in the transgenic adenocarcinoma of the mouse prostate (TRAMP) derived TRAMP-C2 model. Immunofluorescence imaging showed that TH-302 drives an influx of T cells into hypoxic zones, which were expanded by checkpoint blockade. Further, combination therapy reduced myeloid-derived suppressor cell density by more than 50%, and durably reduced the capacity of the tumor to replenish the granulocytic subset. Spontaneous prostate tumors in TRAMP transgenic mice, which completely resist checkpoint blockade, showed minimal adenocarcinoma tumor burden at 36 weeks of age and no evidence of neuroendocrine tumors with combination therapy. Survival of *Pb-Cre4, Pten*$^{pc-/-}$*Smad4*$^{pc-/-}$ mice with aggressive prostate adenocarcinoma was also significantly extended by this combination of hypoxia-prodrug and checkpoint blockade. Hypoxia disruption and T cell checkpoint blockade may sensitize some of the most therapeutically resistant cancers to immunotherapy.

Introduction

We have shown previously that antibody blockade of the T cell immune checkpoint receptors CTLA-4 and PD-1 synergized in curing mice of pre-implanted B16 melanoma(1). In clinical trials, more than 50% of metastatic melanoma patients receiving this combination therapy achieved objective clinical responses with the majority experiencing more than 85% reduction in tumor burden(2). For melanoma patients, immunotherapy now offers the hope of durable remissions and even lifelong cures in a setting where therapeutic success was previously defined by a few months of extended survival. For patients suffering from more therapeutically-resistant solid tumors such as castration resistant prostate cancer, pancreatic cancer, and non-hypermutated colorectal cancer; however, no such curative hope exists as T cell checkpoint blockade shows little efficacy(3, 4). Our studies of murine tumor models of prostatic adenocarcinoma suggest that, unlike melanoma, these tumors effectively prevent accumulation of tumor-specific T cells through establishment of inaccessible hypoxic cores, recruitment of myeloid suppressor cells, and establishment of dense stromal barriers lacking in relevant tumor antigens. Tumor hypoxia, in particular, predicts poor outcome across all cancers(5), and serves as a center for recruitment, polarization, and expansion of immune suppressive stromal cell populations(6-9). For prostate cancer, increased hypoxia has been shown to strongly correlate with more aggressive disease (10), and to be both prevalent and severe in prostate patients (11).

Antibodies that block T cell co-inhibitory receptors or activate co-stimulatory ones can potently reverse T cell anergy and suppression in “hot” tumors with pre-existing immune infiltrates; however, immunotherapy performs poorly in “cold” tumors in which T cells are sparse or absent from the tumor microenvironment. We find few, if any, T cells infiltrating the hypoxic areas of either transplantable or spontaneous syngeneic models of prostate cancer. Hypoxia acts both directly (e.g. HIF-1α-mediated upregulation of VEGF) and indirectly (recruitment of cells which promote abnormal angiogenesis) to promote dysregulated tumor angiogenesis. The resulting vasculature expresses little of the adhesion molecules necessary to support T cell extravasation

and can be programmed by hypoxia-induced factors to actively induce apoptosis of T cells via FAS receptor engagement (12). Those T cells that are able to enter hypoxic tumors face a metabolically hostile and highly suppressive environment characterized by acidic pH, depletion of essential amino acids and nutrients (e.g. arginine, tryptophan, glucose), dense expression of inhibitory ligands (e.g. PD-L1), extracellular adenosine, and high concentrations of suppressive cytokines (e.g. TGF-β)(13). In addition, hypoxia drives recruitment of immature myeloid cells, and fosters their phenotypic conversion into highly suppressive MDSC and TAM (6). Thus, hypoxia plays a prominent role in both the establishment and maintenance of tumor immune privilege.

We chose to utilize the hypoxia-activated prodrug, TH-302 (Evofosfamide), as a mechanism for disruption of tumor hypoxia. TH-302 is non-lymphotoxic in animal studies and clinical trials, and we find that it can be administered concurrently with immunotherapy without harming the anti-tumor T cell response (14). Critically, we have observed that hypoxia is reduced, and tumor vasculature normalizes after TH-302 treatment. Hypoxia reduction and checkpoint blockade combine to cure 80% of animals implanted with TRAMP-C2 prostate cancer. We find that this hypoxia-targeted therapy promotes a dramatic and durable decline in MDSC in the tumor, which acts in concert with checkpoint blockade to promote elevated CD8 to MDSC ratios and tumor elimination. In mice receiving TH-302 with T cell checkpoint blockade, CD8 T cell proliferation (Ki67), cytotoxic potential (Granzyme B), activation (CD44) and effector cytokine production (IFN-γ and TNF-α) all increase. At the same time proliferation of granulocytic MDSC in hypoxic zones of prostate tumors decreases, as does their capacity to suppress T cell proliferation.

TRAMP transgenic mice develop tumors in the dorsolateral prostate, which metastasize to the periaortic nodes and lungs, with occasional metastases to the kidney, adrenal gland, and bone as early as 12 weeks (15). Castration resistance develops at varied rates, but nearly 100% of these animals are fully androgen-independent by 20 weeks (16). On the C57BL/6 background, approximately 80% of these animals develop adenocarcinomas while 20% develop neuroendocrine carcinomas(17). Much like metastatic prostate cancer patients, these mice are entirely resistant to checkpoint blockade. We find, however, that hypoxia ablation combined with checkpoint blockade produces profound therapeutic responses in these animals with most exhibiting low to unmeasurable tumor burden even 3 months after discontinuation of therapy. These findings further illustrate that disruption of hypoxic zones compromises the integrity of the suppressive stromal myeloid network and can sensitize even the most therapeutically resistant pre-clinical model of prostate cancer to T cell checkpoint immunotherapy.

Results

***Hypoxic zones within prostate tumors lack T cells*.** Hypoxia is known to be a common feature of clinical prostate cancer which correlates with poor prognosis(10), and we have found it to be equally pervasive across murine transplantable and spontaneous pre-clinical models (**Supplemental Fig. 1A**). In the TRAMP-C2 model, mice bearing 200-300mm^3 prostate tumors were sacrificed following administration of the hypoxia marking compound pimonidazole and the distribution of T cells within them examined by immunofluorescence imaging. Normoxic zones of these tumors are infiltrated by both CD8 and CD4 T cells, although with a sufficient fraction of $CD4^+FoxP3^+$ Treg cells to functionally suppress the effector populations (**Supplemental Fig. 1B**). In contrast, the hypoxic zones of this same tumor lack substantial infiltration by any type of T cells. Within the more physiologic setting of spontaneous prostate cancer in TRAMP transgenic mice, we find that, just as in TRAMP-C2, T cells are largely excluded from hypoxic

zones(**Supplemental Fig. 1C**). This lack of T cell infiltration of hypoxic zones led us to hypothesize that they may serve as islands of immune privilege and, potentially, immunotherapy resistance, within the tumor microenvironment of these cancers.

Targeted hypoxia reduction cooperates with T cell checkpoint blockade to promote rejection of TRAMP-C2 prostate tumors. To test the hypothesis that reduction of hypoxia might reduce prostate cancer immune resistance, we utilized the hypoxia-activated prodrug compound TH-302 as a non-lymphotoxic means to reduce hypoxia. TH-302 is cytotoxic within hypoxic zones of tumors; however, as we found little or no T cells in these areas, we did not anticipate bystander T cell killing. In addition, TH-302 has an exceptionally short *in vivo* half-life and selectively kills proliferating cells, whereas we find little proliferation among the few T cells persisting under hypoxia. Mice were implanted with sub-cutaneous TRAMP-C2 tumors and treated with either combination antibody blockade of the CTLA-4 and PD-1 immune checkpoint receptors, TH-302 hypoxia-activated prodrug, or the prodrug/checkpoint combination in 2 cycles starting 7 days later (**Supplemental Fig. 2A**). The combination of TH-302 with αCTLA-4/αPD-1 (OS 82%) demonstrated therapeutic superiority to TH-302 alone ($p<0.001$; OS 30%) and to dual antibody alone ($p=0.016$; OS 55%) (**Fig. 1A**). The same hierarchy of efficacy was reflected in measurements of tumor growth ($p<0.0001$ for combination versus each monotherapy). We chose to focus on the combination of TH-302 + αCTLA-4/αPD-1 due to its high potential for clinical translation and greater efficacy than TH-302 +αCTLA-4 (OS 50%) or +αPD-1 (OS 30%) alone (**Supplemental Fig. 2B**). The capacity of TH-302 to cure some animals in this study was surprising given its cytotoxic effects are confined to areas of tumor hypoxia. To determine if disruption of these hypoxic zones was catalyzing an immune response capable of eliminating the entirety of the tumor, we repeated these experiments in immune-deficient *Rag* knockout mice and found that neither TH-302 nor the combination could cure any animals (**Supplemental Fig. 2C**). The combination of TH-302 and αCTLA-4/αPD-1 also demonstrated a significant therapeutic benefit in terms of survival ($p=0.02$) and tumor growth control ($p<0.0001$) versus untreated animals against 21-day pre-implanted MyC-CaP prostate tumors (**Supplemental Fig. 2D**) (18, 19). Neither drug nor antibody monotherapy has significant benefit in this model.

While the cytotoxic nature of TH-302 has the potential to boost T cell immunity through tumor and stromal depletion and antigen release from within hypoxic areas, these effects are short-lived and the therapeutic benefit with immunotherapy could not be replicated by substituting the untargeted parental chemotherapy drug, ifosfamide (**Fig. 1B**). Failure of ifosfamide in this context was not due to lymphotoxicity as CD8 T cells from OT-I T cell transgenic mice (Ovalbumin specific) treated for 1 week with ifosfamide (50mg/kg) showed equivalent capacity to expand in response to *ex vivo* peptide stimulation (Ovalbumin-derived SIINFEKL peptide) compared to those from untreated animals(**Supplemental Fig. 2E**). Examination of the full area of slices through TRAMP-C2 tumors following a single cycle of TH-302 therapy revealed prominent hypoxic geography across untreated as well as checkpoint-unresponsive tumors that is profoundly diminished in mice receiving the drug (**Fig. 1C**). Across four full tumors under each condition, we found that more than a third of the area of untreated or antibody treated tumors was hypoxic (**Fig. 1D**). In contrast, mice that received TH-302, alone or in combination with checkpoint blockade, averaged less than 7% hypoxic area across their tumors. We hypothesize that it is the removal of these zones of hypoxia that restores T cell infiltration thereby sensitizing these prostate tumors to checkpoint blockade.

Hypoxia reduction restores T cell access and increases their proliferation within the tumor microenvironment. TRAMP-C2 tumors were established for 14 days, treated with a single cycle of therapy, and then examined for T cell and myeloid cell infiltration of normoxic versus hypoxic areas. As observed previously, T cells are present at low abundance in normoxic tumor areas but absent from hypoxic zones in untreated tumors (**Fig. 2A**). As hypoxic zones break down following TH-302 treatment, the capacity of T cells to extravasate out from vessels in these areas into the tumor tissue may improve (**Fig. 2A**, yellow arrows); however, numbers and depth of infiltrating T cells remain limited likely due to multiple immune suppressive mechanisms including engagement of T cell co-inhibitory pathways. Immune checkpoint blockade drives robust T cell infiltration of normoxic areas of tumor, but very few of these cells can access hypoxic zones of these cancers further supporting their role as centers of therapy resistance. The combination of hypoxia reduction by TH-302 and checkpoint blockade restores the capacity of these T cells to not only infiltrate hypoxic areas but to persist within them and promote tumor elimination (**Fig. 2A**, lower right). These differences are quantified across 10 fields per condition showing that infiltration of hypoxic areas is impaired in the context of checkpoint blockade but not TH-302 monotherapy (**Fig. 2B**). Combination therapy demonstrates significantly elevated normoxic infiltration compared to TH-302 monotherapy and elevated hypoxic infiltration relative to checkpoint blockade. Reduction of hypoxia and restoration of T cell infiltration with the TH-302 and checkpoint blockade combination correlates with increases in the density of $CD31^+$ vessels within these zones (**Supplemental Fig. 3A and B**). These healthier, more complete vessels are likely responsible for both re-oxygenation of the tissue and reduction of hypoxia, as well as potentially for improved T cell extravasation capacity.

In order to assess the impact of hypoxia reduction on the tumor microenvironment as a whole, we established TRAMP-C2 tumors for 2 weeks, treated them with 2 cycles of therapy, and then dissociated their tumors and examined the immune infiltrates by flow cytometry. Even waiting 14 days to begin treatment, combination therapy eliminated tumor in more than 60% of animals making isolation of sufficient numbers of tumors for analysis challenging (**Supplemental Fig. 4**). The flow cytometry gating strategy used in analysis of these tumors, as well as relevant control gating is shown in **Supplemental Fig.** 5. While the ratios of CD8 T cells to suppressive Treg cells improve with immunotherapy in these tumors, the magnitude of that increase is small in comparison to more immunogenic cancers like melanoma (**Fig. 2C**) (1, 20, 21). Importantly, the addition of TH-302 to checkpoint blockade does nothing to impair the benefit of checkpoint blockade on T cell infiltration (**Fig. 2C**). Within untreated TRAMP-C2 tumors, there is approximately 1 Treg cell for every 2 CD8 effector T cells; however, there are also approximately 2 Arginase-positive myeloid derived suppressive cells (MDSC) for every CD8 cell – a potentially far greater impediment to tumor immunity (**Fig. 2D**). Checkpoint blockade or TH-302 only minimally impact this suppressive state, while the combination demonstrates significant synergy by increasing the CD8 to MDSC ratio to 5:1 (**Fig. 2C**). We hypothesize that it is the release from MDSC-mediated suppression that allows CD8 T cells to expand more freely in these tumors.

Hypoxia reduction diminishes suppressive myeloid density in the tumor microenvironment. Unlike T cells, we found $CD11b^+GR\text{-}1^+$ MDSC, as well as $CD11b^+GR\text{-}1^-F4/80^+$ tumor associated macrophages (TAM) to reside in high densities within hypoxic zones of TRAMP-C2 tumors (**Fig. 3A, Supplemental Fig. 6A**). As hypoxic zones diminish following TH-302, density of MDSC within these areas is noticeably diminished. Following combination therapy, this loss of $CD11b^+GR\text{-}1^+$ cells is even more pronounced. In comparison to MDSC

density, macrophage density within these areas remains relatively consistent (**Fig. 3A, Supplemental Fig. 6A**). The tendency of MDSC and suppressive, M2-polarized TAM to concentrate in hypoxic zones of tumors has been described; therefore, we sought to determine the global impact of loss of MDSC from hypoxia on overall tumor MDSC density (6, 22).

Two-week established TRAMP-C2 tumors were treated with 2 cycles of therapy and then their immune infiltrates analyzed by flow cytometry. Across five independent experiments, hypoxia-activated prodrug therapy alone reduced the frequency of $CD11b^{+}Gr\text{-}1^{+}$ MDSC to 0.64 relative to untreated tumors, with the addition of immunotherapy further reducing this frequency to 0.51 (**Fig. 3B**). While MDSC have multiple mechanisms of T cell suppression, production of the enzyme Arginase I is arguably the most potent as T cells are exceptionally sensitive to concentrations of extracellular arginine. The frequency of Arginase-expressing MDSC declines to 0.83 of its baseline with TH-302 alone and is further reduced to 0.51 with combination therapy (**Fig. 3B**). Pooling and analyzing the individual mice rather than the experimental means from these 5 experiments also shows significant MDSC and $Arginase^{+}$ MDSC reduction with TH-302 or the TH-302 and checkpoint blockade combination (**Supplemental Fig. 6B**). In some experiments, the level of $Arginase^{+}$ MDSC appears elevated relative to baseline in mice receiving checkpoint blockade alone, suggesting a potential mechanism of adaptive immune resistance. Absolute densities of $CD11b^{+}Gr\text{-}1^{+}$ MDSC or $Arginase^{+}$ MDSC are reduced to approximately 25% of their density in untreated tumors with hypoxia-activated pro-drug therapy, and, in this case, no further reduction is achieved by the addition of checkpoint blockade (**Fig. 3C**).

***Combined hypoxia reduction and checkpoint blockade decreases MDSC suppressive capacity and promotes T cell effector function*.** We next sought to dissect the impact of TH-302 and checkpoint blockade therapy on the functional properties of T cells, MDSC, and tumor cells within TRAMP-C2 prostate tumors. Twenty-one day established TRAMP-C2 tumors were treated with a single cycle of TH-302 and checkpoint blockade and then their tumor infiltrating T cells and myeloid cells were analyzed by flow cytometry. Granulocytic MDSC proliferation (Ki67) decreased significantly in hypoxic zones of combination treated versus untreated TRAMP-C2 tumors (**Fig. 4A**). This finding is consistent with the overall reductions in this population noted in **Fig. 3**. Total MDSC were isolated from these TRAMP-C2 tumors and tested for their capacity to inhibit the proliferation of CFSE-labelled, polyclonally-activated T cells (αCD3/αCD28). MDSC isolated from tumors that had been treated with TH-302 and blockade of CTLA-4 and PD-1 showed reduced ability to inhibit T cell proliferation relative to Gr-MDSC from untreated tumors (**Fig. 4B**). Thus, combined hypoxia reduction and checkpoint blockade reduces proliferation and suppressive function of tumor-resident MDSC.

To investigate the impact of hypoxia reduction on the functional state of T cells across the tumor microenvironment as a whole, we established TRAMP-C2 tumors for 2 weeks, treated them with 2 cycles of therapy, and then analyzed their immune infiltrates by flow cytometry. By examining the proliferation marker Ki67, we found that the fraction of CD4 effector and CD8 T cells proliferating in these tumors doubled following combination therapy (**Fig. 4C**). In addition, cytotoxic potential of the CD8 T cells in these tumors increased significantly in combination treated animals as measured by both elevated per cell production of Granzyme B or by increases in the percentage of Granzyme B positive cells (**Fig. 4D**). Although Granzyme B less commonly contributes to actual cytotoxicity in CD4 T cells, its expression in this compartment is

associated with heightened activation and is also elevated with hypoxia reduction and checkpoint blockade (**Supplemental Fig. 7A**).

Recently, a critical role for the rate of T cell apoptosis in determining success versus failure of anti-tumor immunity has been demonstrated(23). As T cells face numerous apoptotic stimuli under hypoxia(13), we sought to determine whether hypoxia reduction and checkpoint blockade improved their survival in this environment. Mice were implanted with TRAMP-C2 tumors in 30% Matrigel and treated beginning on day 21 for 1 cycle of therapy. The day after conclusion of therapy, mice were injected with pimonidazole (Hypoxyprobe) and euthanized 6 hours later so that hypoxia exposed versus unexposed populations could be discriminated. Purified CD8 T cells from hypoxic areas of prostate tumors showed high level staining for activated Caspase 3 (a hallmark of apoptotic death), while those from mice treated with TH-302 and checkpoint blockade evidenced significantly lower levels of cell death (**Fig. 4E**).

Significant percentages of CD8 T cells resident in the tumor microenvironment are bystanders lacking in tumor-specificity and capacity to productively contribute to tumor immunity (24). To determine changes in functional phenotype of largely tumor-specific CD8 T cells, we analyzed those expressing significant levels of the co-stimulatory molecule 4-1BB (25). TRAMP-C2 tumor-bearing mice were treated with a single cycle of therapy as above, CD8 T cells were isolated and activated with the Leukocyte Activation Cocktail with Golgi Plug (BD Biosciences) for 5 hours, and then the 4-1BB expressing subset was analyzed by flow cytometry. Hypoxia reduction and checkpoint blockade resulted in heighted activation in this tumor-specific CD8 T cell subset based on CD44 expression (**Fig. 4F**). Consistent with the overall CD8 population, these 4-1BB expressing CD8 T cells also proliferated more robustly (**Supplemental Fig. 7B**). Production of the effector cytokines IFN-γ and TNF-α was also significantly enhanced in tumors from TH-302 and αCTLA-4/αPD-1 treated mice (**Fig. 4G**). Overall, hypoxia reduction combined with checkpoint blockade qualitatively improved the tumor-specific CD8 T cell compartment in terms of activation, proliferation and effector cytokine production.

Hypoxia can suppress T cell metabolism in numerous ways that impair overall anti-tumor immunity (26). We isolated T cells from TRAMP-C2 prostate tumors treated with a single cycle of TH-302 and checkpoint blockade and assayed their mitochondrial function and mass by flow cytometry using MitoTracker Red FM (a cell-permeable red fluorescent dye whose accumulation depends on mitochondrial membrane potential) and their glycolytic potential by measuring glucose uptake using fluorescent 2-NBD-glucose (2-NBDG). Both CD8 and CD4 T cells showed signs of increased mitochondrial respiration, but with unchanged (CD4) or slightly reduced (CD8) glycolytic activity (**Supplemental Fig. 7C, D**). While glycolysis can promote enhanced T cell cytotoxicity, multiple lines of evidence suggest improved T cell function and anti-tumor potential correlates with enhanced mitochondrial respiration and oxidative phosphorylation (27-29).

Having seen that hypoxia reduction and checkpoint blockade reduced the proliferation and suppressive capacity of MDSC while augmenting the activation and effector function of T cells, we sought to examine the impact of therapy on the TRAMP-C2 prostate tumor cells themselves. We implanted tumors and analyzed them under the same conditions as above, and found that long after all TH-302 had cleared, tumor cell proliferation was significantly diminished in the remaining hypoxic zones of these cancers (**Supplemental Fig. 7E**). In sum, TH-302 and checkpoint blockade diminished MDSC and tumor proliferation while increasing expansion of highly functional intra-tumoral T cell populations.

Reduction of tumor hypoxia impairs the capacity of prostate tumors to replenish their suppressive myeloid stroma. Tumors recruit immature myeloid cells and polarize them to become suppressive MDSC and TAM via a variety of factors enriched in hypoxic microenvironments including VEGF, reactive oxygen species, TGF-β, IL-6, prostaglandin E2, GM-CSF and G-CSF(30, 31). We hypothesized that loss of hypoxic zones might, therefore, compromise the capacity of prostate tumors to recruit and suppressively polarize new myeloid stroma. To test this, we established large TRAMP-C2 tumors (32d), treated them with a single cycle of therapy, adoptively transferred immature bone-marrow myeloid cells from congenically-marked mice, and then examined the frequency and phenotype of these cells within the previously treated tumors 60 hours post-transfer. Mice which had been previously treated with hypoxia prodrug and checkpoint blockade were only half as efficient at polarizing the adoptively transferred myeloid progenitors into granulocytic MDSC (Gr-MDSC) relative to untreated animals (0.53x Gr-MDSC of $CD45.1^+$ myeloid; p=0.001) (**Fig. 5A**). Further, the cells which bear the markers of Gr-MDSC ($CD11b^+Ly6G^+Ly6C^-F4/80^-$) in the combination treated animals showed incomplete suppressive polarization as they failed to fully upregulate Arginase I (0.79x MFI; p=0.03) and to downregulate MHC II expression (2.03x MFI; p=0.003) (**Fig. 5B**). These data suggest long-term defects in the capacity of these tumors to replenish their granulocytic MDSC compartment, which could be related to persistent loss of hypoxia. We hypothesize that the lack of defect in Gr-MDSC polarization in mice receiving TH-302 alone versus the combination in this setting may reflect re-establishment of hypoxia over the week prior to analysis in which these mice receive no drug versus maintenance of hypoxia reduction by the expanded pro-inflammatory immune infiltrate in the presence of checkpoint blockade.

Hypoxia reduction sensitizes spontaneously arising prostate tumors to checkpoint blockade. Prostate tumors in TRAMP mice develop in the dorsolateral prostate and metastasize to the periaortic nodes and lungs, with occasional metastases to the kidney, adrenal gland, and bone as early as 12 weeks (15). TRAMP mice develop castration resistance at varied rates but nearly 100% are fully androgen-independent by 20 weeks (16). On the B6 background, TRAMP mice develop approximately 80% adenocarcinomas and 20% neuroendocrine tumors, but if moved to a B6/FVB F1 background will develop 100% neuroendocrine cancers(17). We waited until 16 weeks of age to begin treating TRAMP mice (B6 background) at which point they have carcinoma *in situ* as well as local metastatic disease in most animals. Mice were treated with 3 cycles of therapy and then followed until 36 weeks of age, at which point they were sacrificed and their prostates weighed to assess tumor burden. When all tumors, both neuroendocrine (triangles) and adenocarcinomas (circles) are considered, as well as all mice regardless of whether they lived to 36 weeks (red indicates death prior to 36 weeks), it is apparent that checkpoint blockade has no impact on tumor progression in this model of prostate cancer (**Fig. 6A**). Due to the rapid progression of neuroendocrine tumors, we were not able to obtain tumor weights for some animals that died prior to 36 weeks and represented tumors from these animals at the average weight of all neuroendocrine tumors that we were able to measure (5157mg). While TH-302 appears to slow the progression of adenocarcinomas in this setting, it has no impact on neuroendocrine disease. The combination of TH-302 and blockade of CTLA-4 and PD-1, however, has a striking therapeutic effect with all animals showing tumor control or modest levels of progression at 36 weeks ($p \leq 0.001$ compared to all groups). This degree of tumor control more than 3 months after the end of therapy is unprecedented in this model. When this study is limited only to mice

with adenocarcinomas and only to mice that survive to the 36-week sacrifice, a condition that under-represents TH-302 tumor sizes as many more of those animals die < 36 weeks compared to combination treatment, it remains clear that the combination of hypoxia-targeted therapy and checkpoint blockade (877.6mg) controls tumor progression in this model better than checkpoint blockade alone (2227mg; $p<0.0001$) or TH-302 alone (1470mg; $p=0.0099$) (**Fig. 6B**).

While neuroendocrine (NE) tumors are known to develop less frequently in the TRAMP model than adenocarcinomas (~20% NE), they develop sooner and progress more rapidly. Between the antibody, TH-302, and untreated TRAMP mice, we observed 23 NE tumors versus 58 adenocarcinomas, which represents an insignificant deviation from the predicted frequency based on the published data (**Fig. 6C**). On the other hand, in 23 mice treated with the combination of TH-302 and dual checkpoint blockade, we have yet to observe a single NE tumor. This highly significant ($p<0.001$) underrepresentation of neuroendocrine disease in this group relative to both expected norms and to our observed frequency in the other groups, suggests that combination therapy can slow and/or block the progression of these tumors, and may even be able to eliminate them altogether.

TRAMP prostate cancer grows diffusely throughout the prostate making it impossible to grossly distinguish tumor from normal tissue. With this caveat in mind, we analyzed the prostate-infiltrating lymphocytes of TRAMP mice sacrificed at the 36-week time point above from three independent experiments. Even nearly 4 months after their last treatment, TRAMP mice that had received TH-302 and CTLA-4/PD-1 blockade showed elevated ratios of both CD8 to Treg and CD4 Teff to Treg in their prostates (**Fig. 6D**). While there was a slight trend toward elevated CD8 to MDSC ratios in the combination-treated animals as well, these differences were no longer significant so far removed from treatment (**Supplemental Fig. 8A**). To test the more immediate impact of therapy in these animals, we treated 30-week old TRAMP mice with TH-302 and checkpoint blockade for 9 days and then isolated and analyzed their prostate-infiltrating lymphocytes at day 11 (n=2, 3m/group). In this setting, we observed trends toward higher CD4 and CD8 T cell proliferation in the treated mice consistent with our observations in TRAMP-C2 (**Supplemental Fig. 8B**). In addition, we observed a significant drop in Mo-MDSC proliferation and trends toward reduced Gr-MDSC and TAM expansion (**Supplemental Fig. 8C**). While also not statistically significant with the numbers of animals available, CD8 to MDSC ratios in this setting appeared to improve with treatment (**Supplemental Fig. 8D**). Overall, hypoxia reduction and checkpoint blockade appeared to durably improve effector T cell to suppressive Treg ratios in TRAMP prostates, and showed signs of MDSC reduction and T cell expansion that mirrored our observations in the TRAMP-C2 model.

Mice bearing the *Pb-Cre4, Pten*$^{pc-/-}$*Smad4*$^{pc-/-}$ genotype develop aggressive, invasive adenocarcinoma of the prostate by 11 weeks of age and nearly all die by 32 weeks of age(32). We sought to evaluate the impact of combination checkpoint blockade and hypoxia reduction in these animals that develop tumors with earlier onset and more rapid progression than TRAMP mice due to the distinct molecular drivers in this model. Mice were treated starting at 12 weeks of age for 3 cycles of therapy (last treatment day 115) and then monitored for survival. Combination-treated animals showed significantly improved survival versus untreated animals (**Fig. 6E**). The therapeutic effect in these animals was pronounced during therapy and for some time after; however, over time, these animals progress with a kinetic approaching that of untreated mice. This progression following discontinuation of therapy is likely due to rapid emergence of new tumors in this model that lack significant antigenic identity with their original

disease, and, thus, are immune to memory T cell responses generated during the first round of therapy.

Discussion

A major impediment to widespread efficacy of T cell immune checkpoint blockade is the lack of T cell infiltration observed in “cold” tumors which has been associated with poor prognosis(33). Similarly, hypoxia has been associated with poor prognosis in prostate cancer and many other tumors (5, 10, 34). We report that hypoxic zones of prostate tumors represent centers of immune and immunotherapy resistance from which T cells are largely excluded, even in the context of combination checkpoint blockade. Using the hypoxia prodrug TH-302 to reduce tumor hypoxia and potentially also release tumor antigen, we show that hypoxia reduction increases the sensitivity of TRAMP-C2 tumors to checkpoint blockade. We find that TH-302 shows little cooperativity with αPD-1 alone; however, the addition of αPD-1 to αCTLA-4 augments anti-tumor immune responses. We interpret this data to show that depletion of Tregs and enhancement of T cell priming and expansion are necessary pre-requisites to elicit sufficient tumor infiltration by PD-1^+ effector T cells to reveal benefit with PD-1 blockade. Unlike TRAMP-C2, which does respond well to checkpoint blockade alone, spontaneous prostate tumors in TRAMP mice are completely unresponsive to CTLA-4/PD-1 blockade reflecting the lack of response of metastatic prostate cancer patients. In this setting, hypoxia ablation potently sensitizes TRAMP tumors to checkpoint blockade with mice demonstrating low to absent tumor burden even 4 months after withdrawal of therapy. Especially given the advanced stage of disease at which therapy was initiated in these animals, the therapeutic efficacy of this combination provides a strong rationale for clinical translation.

Suppressive myeloid cells, particularly MDSC, concentrate in hypoxic zones in these tumors and form a potent barrier to tumor immunity. Reduction of hypoxia with TH-302 not only has an immediate effect on diminishing MDSC frequency and density within these tumors, but also causes persistent defects in the capacity of these tumors to replenish their suppressive myeloid stroma through recruitment and suppressive polarization of new granulocytic MDSC. Further, we find that the capacity of the remaining MDSC to suppress T cells in mice receiving the TH-302 and checkpoint blockade combination is reduced. Loss of this immune inhibitory barrier reverses the highly suppressive ratio of MDSC to CD8 T cells present in untreated tumors, allows these T cells to infiltrate and survive in formerly hypoxic areas from which they were excluded, and allows the infiltrating effector T cells to proliferate at twice their prior rate. CD8 T cells in combination-treated tumors also show higher Granzyme B expression, higher proliferation and CD44 expression, and greater effector cytokine production. These T cells appear to evade killing by the drug due to their absence from areas of deep hypoxia, relatively low proliferation absent checkpoint blockade, and capacity to infiltrate hypoxic areas only as they are breaking down and becoming less competent to activate TH-302. Also, both ifosfamide (which shares the active moiety of TH-302) and the related chemotherapeutic, cyclophosphamide, have demonstrated preferential cytotoxicity for Treg while sparing effector T cells (35, 36). Further investigation is warranted to determine whether this mechanism translates to other hypoxic tumors that rely on suppressive myeloid stroma to mediate T cell exclusion and immunotherapy resistance such as pancreatic cancer and head and neck cancer, particularly the highly hypoxic basal subtype.

An earlier study demonstrated that inhaled hyperoxia was also able to sensitize lung tumors to immune checkpoint blockade (37). We find this study highly supportive of our findings, although

their mechanistic focus was on reduction of immune suppressive extracellular adenosine levels. We plan to investigate the role of adenosine reduction in response to hypoxia reduction in our system in the future, including whether some of the myeloid cell populations that are diminished are contributing to adenosine accumulation. Another highly supportive study was recently published showing a limited capacity of metformin to reduce tumor hypoxia and thereby sensitize a number of murine transplantable tumors to PD-1 blockade(38).

We demonstrate the capacity of targeted hypoxia reduction to sensitize multiple pre-clinical models of prostate cancer to T cell checkpoint blockade; however, we have not yet directly addressed the clinical potential of this approach. A recent study of gene signatures that correlate with resistance to PD-1 antibody therapy in melanoma patients found that hypoxia gene sets were enriched in non-responding patients (39). These observations further support clinical investigation of hypoxia ablation as a mechanism to overcome lack of response to checkpoint blockade. We have therefore opened a Phase I clinical trial to explore the capacity of the combination of TH-302 and Ipilimumab in this regard at our institution across a number of checkpoint-resistant indications (NCT03098160).

Materials and Methods

Animals

Eight-week old male C57BL/6, FVB/N and B6.RAG$^{-/-}$ mice were purchased from the Jackson Laboratory. The animals were maintained in a specific-pathogen free environment at the institutional animal facility. All procedures were conducted in accordance with the guidelines established by the U.T. MD Anderson Cancer Center Institutional Animal Care and Use Committee. TRAMP transgenic mice were also purchased from the Jackson Laboratory, maintained as homozygotes, and then bred to C57BL/6 mice to generate heterozygous progeny used in experiments. *Pb-Cre4, Pten$^{pc-/-}$Smad4$^{pc-/-}$* mice were kindly provided by the laboratory of Dr. Ronald DePinho. At various experimentally indicated time points post tumor challenge and/or immunization, animals were sacrificed according to institutional guidelines.

Cell Lines and Reagents

The TRAMP-C2 tumor cell line was provided by Dr. Norman Greenberg and all experiments in this manuscript were performed using passage 21-22 tumor cells. TRAMP-C2 cells were maintained as previously described (40). The MyC-CaP cell line was obtained directly from ATCC (ATCC® CRL-3255™) and used at passage 3 from that stock for all studies.

Therapeutic antibodies and drugs

Therapeutic antibodies were purchased from BioXcell at <1EU/mg of LPS and included hamster anti-mouse CTLA-4 (9H10 at 100µg/dose) and rat anti-mouse PD-1 (RMP1-14 at 250µg/dose). TH-302 was provided by Threshold Inc., prepared each week in 1x phosphate buffered saline solution, and used at a dose of 50mg/kg. Ifosfamide was prepared using the same protocol and dosing (50 mg/kg).

Prostate tumor treatment experiments

Mice were injected with a single-cell suspension of 1 X 10^6 TRAMP-C2 cells/animal subcutaneously (SC) on the right flank as described previously(41). For MyC-CaP, 2x10^5 cells were injected and treatment was initiated at day 21. For tumor infiltrate analysis experiments,

TRAMP-C2 cells were implanted in 30% Matrigel (Corning). Mice receive TH-302 at 50mg/kg/day i.p. for 5 straight days beginning 7 days following implantation for TRAMP-C2 treatment studies. CTLA-4 and PD-1 blocking antibodies were administered i.p. on days 1, 4, and 7 of each TH-302 cycle. For TRAMP-C2 and MyC-CaP therapeutic and analytic experiments, mice received 2 cycles of therapy with a week of rest in between, while TRAMP and *Pb-Cre4, Pten*$^{pc-/-}$*Smad4*$^{pc-/-}$ spontaneous prostate tumor mice received 3 cycles of therapy each with a week of rest in between beginning at 16 weeks of age for TRAMP and 12 weeks of age for *Pb-Cre4, Pten*$^{pc-/-}$*Smad4*$^{pc-/-}$.

For TRAMP-C2 and MyC-CaP, tumor growth was measured using a caliper to determine the diameter: longest surface length (a) width (b), and depth (c), and tumor size was expressed as volume (a x b x c). Mice were euthanized when the tumor volume reached 1000mm^3. TRAMP transgenic mice are monitored until 36 weeks of age at which point they are sacrificed and their prostates weighed to assess tumor burden. For mice which died or demonstrated distress or undue tumor burden prior to 36 weeks of age, every effort was made to recover tumor in a timely fashion for weighing, and all mice were grossly examined to determine whether they carried adenocarcinomas or neuroendocrine carcinomas.

Adoptive transfer of immature myeloid cells

TRAMP-C2 tumors were implanted as described above. 32 days post-implantation (tumor size 100-250mm^3), animals were treated, or left untreated, for one cycle of therapy and then rested for an additional 2 days. CD11b$^+$CD3$^-$CD19$^-$ immature myeloid cells were isolated from the bone marrow of B6.SJL mice (Jackson Laboratory) by fluorescence activated cell sorting (FACS) using a BD Aria III. 2x10^6 CD45.1$^+$ cells were then injected i.v. into the CD45.2$^+$ TRAMP-C2 tumor bearing mice. 60 hours later, TRAMP-C2 tumors were isolated from these mice and analyzed by flow cytometry with the transferred cells identified as CD45.1$^+$.

Tumor infiltrating lymphocyte isolation

On day 30 post s.c. tumor challenge, mice were sacrificed and tumors were harvested to characterize cell-mediated anti-tumor responses. Briefly, tumors were digested in X-Vivo-15 (Lonza) supplemented with Collagenase H (Sigma) and DNAse (Roche) and incubated at 37ºC, 5% CO2 for 30 minutes before being filtered through a 70 µm cell strainer. Viable immune cells were enriched through density gradient separation over Histopaque 1119 (Sigma) with a short spin (10') at 1000g to minimize loss of myeloid populations. Average CD45$^+$ cell percentage post-Ficoll for untreated TRAMP-C2 tumors (n=20) with this protocol is 8.5% of viable singlets by flow cytometry. For cell density calculations, samples are counted for viable single cells following disruption but prior to Ficoll separation on a ViCell counter (Millipore). The percentage of total cells of a given population measured by flow cytometry is then multiplied back against the total cell count to give the total number of those cells. This number is then divided by the mass to derive density (number of cells per mg of tumor).

Flow cytometry analysis

Samples were fixed using the Foxp3 / Transcription Factor Staining Buffer Set (Affymetrix) and then stained with up to 18 antibodies at a time from Biolegend, BD Biosciences, Affymetrix, Santa Cruz, and Fisher. Flow data was collected on a 5-laser, 18-color BD LSR II cytometer and analyzed using FlowJo Version 7.6.5 (Treestar).

Immunofluorescence staining and imaging

Mouse tissues were collected and embedded in Tissue-Tek® OCT Compound (Sakura, Torrance, CA). The embedded tissues were then flash frozen in liquid nitrogen and sectioned at the MD Anderson Histology Core. The sectioned tissue was fixed with acetone for 10 min, permeabilized with the FoxP3 staining kit (eBioscience, San Diego, CA) for 10 min and blocked with Superblock (ThermoFisher) for 15 min at room temperature. The samples were stained with antibodies in 2% bovine serum albumin, 0.2% Triton-X100 in PBS at room temperature for 30 min and, after being washed in PBS, mounted with Prolong® Gold anti-fade reagent (Invitrogen, Carlsbad, CA). For imaging hypoxia, mice were administered Pimonidazole (Hypoxyprobe, Burlington, MA) intravenously three to six hours prior to euthanasia so that hypoxia could be imaged in tumor sections by immunofluorescence staining with anti-pimonidazole adduct FITC conjugated antibody (Hypoxyprobe, Burlington, MA). Fluorescence microscopy was performed using a TCS SP8 laser-scanning confocal microscope equipped with lasers for 405nm, 458nm, 488nm, 514nm, 568nm, and 642nm wavelengths (Leica Microsystems, Inc., Bannockburn, IL).

For quantitation of CD3+ T cell infiltration into tumors, cells in at least 10 fields per tumor were counted. At least 2 tumors per condition were analyzed. The average CD3+ T cell number per field was calculated.

MDSC Suppression Assay

Mice were injected with a single-cell suspension of 1 X 10^6 TRAMP-C2 cells/animal sub-cutaneously. Beginning 21 days following implantation, mice were treated with TH-302 in combination with αCTLA-4+αPD-1 for 2 cycles of therapy. $CD11b^+Gr\text{-}1^+$ MDSC were sorted from TRAMP-C2 tumors and co-cultured with αCD3/ αCD28 activated T cells for 72 hours. T cell proliferation was measured by CFSE dilution. FlowJo 7.6.5 (Treestar) was used to analyze data.

Metabolic profiling of T cells

Mice were injected with a single-cell suspension of 1 X 10^6 TRAMP-C2 cells/animal subcutaneously. Beginning 21 days following implantation, mice were treated with TH-302 in combination with αCTLA-4+αPD-1 for 1 cycle of therapy. The day after conclusion of therapy, mice were injected with fluorescently labeled glucose, 2-NBDG (Cayman Chemical) i.v thirty minutes before euthanasia and glucose uptake measured by flow cytometry. MitoTracker Deep Red FM staining (Invitrogen) was used to assess total mitochondrial mass.

Characterization of T cell effector function

Mice were injected with a single-cell suspension of 1 X 10^6 TRAMP-C2 cells/animal subcutaneously. Beginning 21 days following implantation, mice were treated with TH-302 in combination with αCTLA-4+αPD-1 for 1 cycle of therapy. The day after conclusion of therapy, mice were euthanized and viable immune cells enriched through density gradient separation over Histopaque 1119 (Sigma). $CD8^+$ T cells were isolated from immune cells via negative selection through magnetic beads using MACS $CD8^+$ T cell isolation kit (Miltenyi Biotec, CA). $CD8^+$ T cells were activated for 5 hours using Leukocyte Activation Cocktail with Golgi Plug (BD Biosciences) and analyzed using flow cytometry. FlowJo 7.6.5 (Treestar) was used to analyze data.

Statistical analysis

Computations for all statistical analyses were conducted in GraphPad Prism Version 6 for Windows and SPSS. One-way ANOVAs were applied to test the differences between multiple groups for continuous variables. Overall survival distributions were estimated using the method of Kaplan and Meier and compared using the Mantel-Cox (Log Rank) test.

For tumor growth curves, the linear mixed model was used to analyze the longitudinal tumor size data with consideration of within-mouse correlations. This model evaluated the time trends of tumor sizes across different treatment groups by including interaction terms between the treatment and time. The proportion test was applied to compare the predicted and observed frequencies of adenocarcinoma and neuroendocrine tumor development in the TRAMP model. Graphs show mean ± SEM unless otherwise indicated. P-values less than 0.05 were considered statistically significant.

Study Approval

All animal studies were approved by the MD Anderson Cancer Center Institutional Animal Care and Use Committee (IACUC, Houston, Texas) under protocol 00001378-RN00/1.

Data availability

All data generated or analyzed during this study are included in this published article (and its supplementary information files). Any reasonable requests for more detailed descriptions of data included herein will be honored by the corresponding author.

Author Contributions

P.J., M.A., A.L. and M.A.C. designed research; P.J., M.A., A.L., T.B., P.B., J.S., C.A., C.N., A.R.J., Y.S., K.S., S.B. and M.A.C. performed research; P.J., M.A., A.L., A.Z., T.Z. and M.A.C. performed confocal imaging and associated analysis; P.J., M.A., A.L., T.B., C.A., C.N. and M.A.C. analyzed data; G.W. provided transgenic animals and untreated survival data; N.L., J.N., P.J., M.A. and M.A.C. performed statistical analyses and power calculations; and P.J., M.A., A.L. and M.A.C. wrote the manuscript.

Acknowledgements

Michael A. Curran was supported in this work by a Cancer Research Institute CLIP Grant and by the MD Anderson Prostate Cancer SPORE (P50 CA140388) Career Development Program. These studies are currently being supported by CPRIT Investigator grant RP170399. The Immunology Imaging Core and Flow Cytometry Core facilities assisted in these studies and are supported by the S10 RR029552 (NIH) and MD Anderson instrumentation grants. Threshold Inc. kindly provided TH-302 for this work as well as consultation on its use.

References

1. Curran MA, Montalvo W, Yagita H, and Allison JP. PD-1 and CTLA-4 combination blockade expands infiltrating T cells and reduces regulatory T and myeloid cells within B16 melanoma tumors. *Proc Natl Acad Sci U S A.* 2010;107(9):4275-80.
2. Wolchok JD, Kluger H, Callahan MK, Postow MA, Rizvi NA, Lesokhin AM, et al. Nivolumab plus ipilimumab in advanced melanoma. *N Engl J Med.* 2013;369(2):122-33.
3. Kwon ED, Drake CG, Scher HI, Fizazi K, Bossi A, van den Eertwegh AJ, et al. Ipilimumab versus placebo after radiotherapy in patients with metastatic castration-resistant prostate cancer that had progressed after docetaxel chemotherapy (CA184-043): a multicentre, randomised, double-blind, phase 3 trial. *Lancet Oncol.* 2014;15(7):700-12.
4. Royal RE, Levy C, Turner K, Mathur A, Hughes M, Kammula US, et al. Phase 2 trial of single agent Ipilimumab (anti-CTLA-4) for locally advanced or metastatic pancreatic adenocarcinoma. *J Immunother.* 2010;33(8):828-33.
5. Saggar JK, Yu M, Tan Q, and Tannock IF. The tumor microenvironment and strategies to improve drug distribution. *Front Oncol.* 2013;3:154.
6. Corzo CA, Condamine T, Lu L, Cotter MJ, Youn JI, Cheng P, et al. HIF-1alpha regulates function and differentiation of myeloid-derived suppressor cells in the tumor microenvironment. *J Exp Med.* 2010;207(11):2439-53.
7. Dang EV, Barbi J, Yang HY, Jinasena D, Yu H, Zheng Y, et al. Control of T(H)17/T(reg) balance by hypoxia-inducible factor 1. *Cell.* 2011;146(5):772-84.
8. Ben-Shoshan J, Maysel-Auslender S, Mor A, Keren G, and George J. Hypoxia controls CD4+CD25+ regulatory T-cell homeostasis via hypoxia-inducible factor-1alpha. *Eur J Immunol.* 2008;38(9):2412-8.
9. Becker JC, Andersen MH, Schrama D, and Thor Straten P. Immune-suppressive properties of the tumor microenvironment. *Cancer immunology, immunotherapy : CII.* 2013;62(7):1137-48.
10. Ragnum HB, Vlatkovic L, Lie AK, Axcrona K, Julin CH, Frikstad KM, et al. The tumour hypoxia marker pimonidazole reflects a transcriptional programme associated with aggressive prostate cancer. *Br J Cancer.* 2015;112(2):382-90.
11. Vaupel P, Hockel M, and Mayer A. Detection and characterization of tumor hypoxia using pO2 histography. *Antioxid Redox Signal.* 2007;9(8):1221-35.
12. Motz GT, Santoro SP, Wang LP, Garrabrant T, Lastra RR, Hagemann IS, et al. Tumor endothelium FasL establishes a selective immune barrier promoting tolerance in tumors. *Nat Med.* 2014;20(6):607-15.
13. Chouaib S, Noman MZ, Kosmatopoulos K, and Curran MA. Hypoxic stress: obstacles and opportunities for innovative immunotherapy of cancer. *Oncogene.* 2016.
14. Duan JX, Jiao H, Kaizerman J, Stanton T, Evans JW, Lan L, et al. Potent and highly selective hypoxia-activated achiral phosphoramidate mustards as anticancer drugs. *J Med Chem.* 2008;51(8):2412-20.
15. Gingrich JR, Barrios RJ, Morton RA, Boyce BF, DeMayo FJ, Finegold MJ, et al. Metastatic prostate cancer in a transgenic mouse. *Cancer Res.* 1996;56(18):4096-102.
16. Tang Y, Wang L, Goloubeva O, Khan MA, Zhang B, and Hussain A. Divergent effects of castration on prostate cancer in TRAMP mice: possible implications for therapy. *Clin Cancer Res.* 2008;14(10):2936-43.
17. Chiaverotti T, Couto SS, Donjacour A, Mao JH, Nagase H, Cardiff RD, et al. Dissociation of epithelial and neuroendocrine carcinoma lineages in the transgenic adenocarcinoma of mouse prostate model of prostate cancer. *Am J Pathol.* 2008;172(1):236-46.

18. Ellwood-Yen K, Graeber TG, Wongvipat J, Iruela-Arispe ML, Zhang J, Matusik R, et al. Myc-driven murine prostate cancer shares molecular features with human prostate tumors. *Cancer Cell.* 2003;4(3):223-38.
19. Watson PA, Ellwood-Yen K, King JC, Wongvipat J, Lebeau MM, and Sawyers CL. Context-dependent hormone-refractory progression revealed through characterization of a novel murine prostate cancer cell line. *Cancer Res.* 2005;65(24):11565-71.
20. Quezada SA, Peggs KS, Curran MA, and Allison JP. CTLA4 blockade and GM-CSF combination immunotherapy alters the intratumor balance of effector and regulatory T cells. *J Clin Invest.* 2006;116(7):1935-45.
21. Curran MA, Kim M, Montalvo W, Al-Shamkhani A, and Allison JP. Combination CTLA-4 blockade and 4-1BB activation enhances tumor rejection by increasing T-cell infiltration, proliferation, and cytokine production. *PLoS One.* 2011;6(4):e19499.
22. Casazza A, Laoui D, Wenes M, Rizzolio S, Bassani N, Mambretti M, et al. Impeding macrophage entry into hypoxic tumor areas by Sema3A/Nrp1 signaling blockade inhibits angiogenesis and restores antitumor immunity. *Cancer Cell.* 2013;24(6):695-709.
23. Horton BL, Williams JB, Cabanov A, Spranger S, and Gajewski TF. Intratumoral CD8(+) T-cell Apoptosis Is a Major Component of T-cell Dysfunction and Impedes Antitumor Immunity. *Cancer Immunol Res.* 2018;6(1):14-24.
24. Simoni Y, Becht E, Fehlings M, Loh CY, Koo SL, Teng KWW, et al. Bystander CD8(+) T cells are abundant and phenotypically distinct in human tumour infiltrates. *Nature.* 2018;557(7706):575-9.
25. Ye Q, Song DG, Poussin M, Yamamoto T, Best A, Li C, et al. CD137 accurately identifies and enriches for naturally occurring tumor-reactive T cells in tumor. *Clin Cancer Res.* 2014;20(1):44-55.
26. Vuillefroy de Silly R, Dietrich PY, and Walker PR. Hypoxia and antitumor CD8(+) T cells: An incompatible alliance? *Oncoimmunology.* 2016;5(12):e1232236.
27. Geiger R, Rieckmann JC, Wolf T, Basso C, Feng Y, Fuhrer T, et al. L-Arginine Modulates T Cell Metabolism and Enhances Survival and Anti-tumor Activity. *Cell.* 2016;167(3):829-42 e13.
28. Sukumar M, Liu J, Ji Y, Subramanian M, Crompton JG, Yu Z, et al. Inhibiting glycolytic metabolism enhances CD8+ T cell memory and antitumor function. *J Clin Invest.* 2013;123(10):4479-88.
29. Scharping NE, Menk AV, Moreci RS, Whetstone RD, Dadey RE, Watkins SC, et al. The Tumor Microenvironment Represses T Cell Mitochondrial Biogenesis to Drive Intratumoral T Cell Metabolic Insufficiency and Dysfunction. *Immunity.* 2016;45(3):701-3.
30. Gabrusiewicz K, Rodriguez B, Wei J, Hashimoto Y, Healy LM, Maiti SN, et al. Glioblastoma-infiltrated innate immune cells resemble M0 macrophage phenotype. *JCI Insight.* 2016;1(2).
31. Marvel D, and Gabrilovich DI. Myeloid-derived suppressor cells in the tumor microenvironment: expect the unexpected. *J Clin Invest.* 2015;125(9):3356-64.
32. Ding Z, Wu CJ, Chu GC, Xiao Y, Ho D, Zhang J, et al. SMAD4-dependent barrier constrains prostate cancer growth and metastatic progression. *Nature.* 2011;470(7333):269-73.
33. Fridman WH, Pages F, Sautes-Fridman C, and Galon J. The immune contexture in human tumours: impact on clinical outcome. *Nat Rev Cancer.* 2012;12(4):298-306.
34. Wilson WR, and Hay MP. Targeting hypoxia in cancer therapy. *Nat Rev Cancer.* 2011;11(6):393-410.
35. Madondo MT, Quinn M, and Plebanski M. Low dose cyclophosphamide: Mechanisms of T cell modulation. *Cancer Treat Rev.* 2016;42:3-9.
36. Brown JS, Sundar R, and Lopez J. Combining DNA damaging therapeutics with immunotherapy: more haste, less speed. *Br J Cancer.* 2018;118(3):312-24.

37. Hatfield SM, Kjaergaard J, Lukashev D, Schreiber TH, Belikoff B, Abbott R, et al. Immunological mechanisms of the antitumor effects of supplemental oxygenation. *Sci Transl Med.* 2015;7(277):277ra30.
38. Scharping NE, Menk AV, Whetstone RD, Zeng X, and Delgoffe GM. Efficacy of PD-1 Blockade Is Potentiated by Metformin-Induced Reduction of Tumor Hypoxia. *Cancer Immunol Res.* 2017;5(1):9-16.
39. Hugo W, Zaretsky JM, Sun L, Song C, Moreno BH, Hu-Lieskovan S, et al. Genomic and Transcriptomic Features of Response to Anti-PD-1 Therapy in Metastatic Melanoma. *Cell.* 2016;165(1):35-44.
40. Foster BA, Gingrich JR, Kwon ED, Madias C, and Greenberg NM. Characterization of prostatic epithelial cell lines derived from transgenic adenocarcinoma of the mouse prostate (TRAMP) model. *Cancer Res.* 1997;57(16):3325-30.
41. Curran MA, and Allison JP. Tumor Vaccines Expressing Flt3 Ligand Synergize with CTLA-4 Blockade to Reject Preimplanted Tumors. *Cancer Res.* 2009;69(19):7747-55.

Figures:

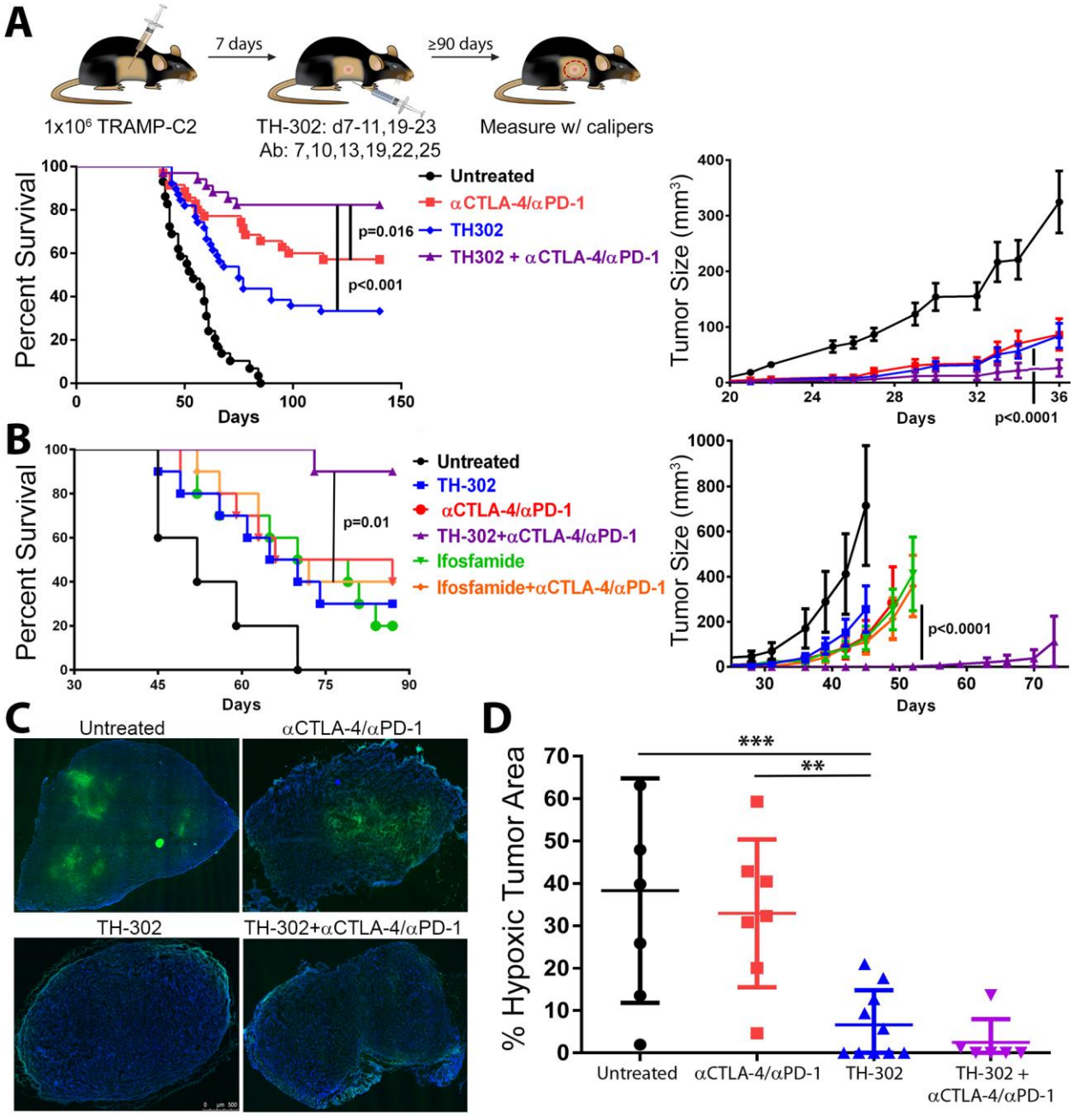

Figure 1. *Hypoxia ablation cooperates with T cell checkpoint blockade to promote rejection of TRAMP-C2 prostate tumors.* (**A**) Mice bearing 7-day pre-implanted TRAMP-C2 tumors were treated with 2 cycles of TH-302 and/or αCTLA-4/αPD-1 antibody and monitored for survival and tumor growth for 140 days (5-10m/group, n=5). Statistical significance for survival was calculated using the log-rank (Mantel-Cox) test and for tumor growth, a linear mixed model was used to analyze the longitudinal tumor size data with consideration of within-mouse correlations. (**B**) Mice bearing 7-day pre-implanted TRAMP-C2 tumors were treated as in **A** except that groups receiving Ifosfamide (50 mg/kg) with or without antibody were included (10m/group [5m/Untreated], n=1). (**C**) TRAMP-C2 tumor-bearing mice were treated with a single cycle of

therapy and 2 days later their tumors were stained for hypoxia following pimonidazole injection (Hypoxyprobe) and imaged at low magnification (10x). Representative images are shown for each group. (**D**) Hypoxic area from 4 full tumor slices for each group were quantified using ImageJ and the statistical significance between groups determined by ANOVA. ns = not significant * = P<0.05, ** = P<0.01, *** = P<0.001, **** = P<0.0001.

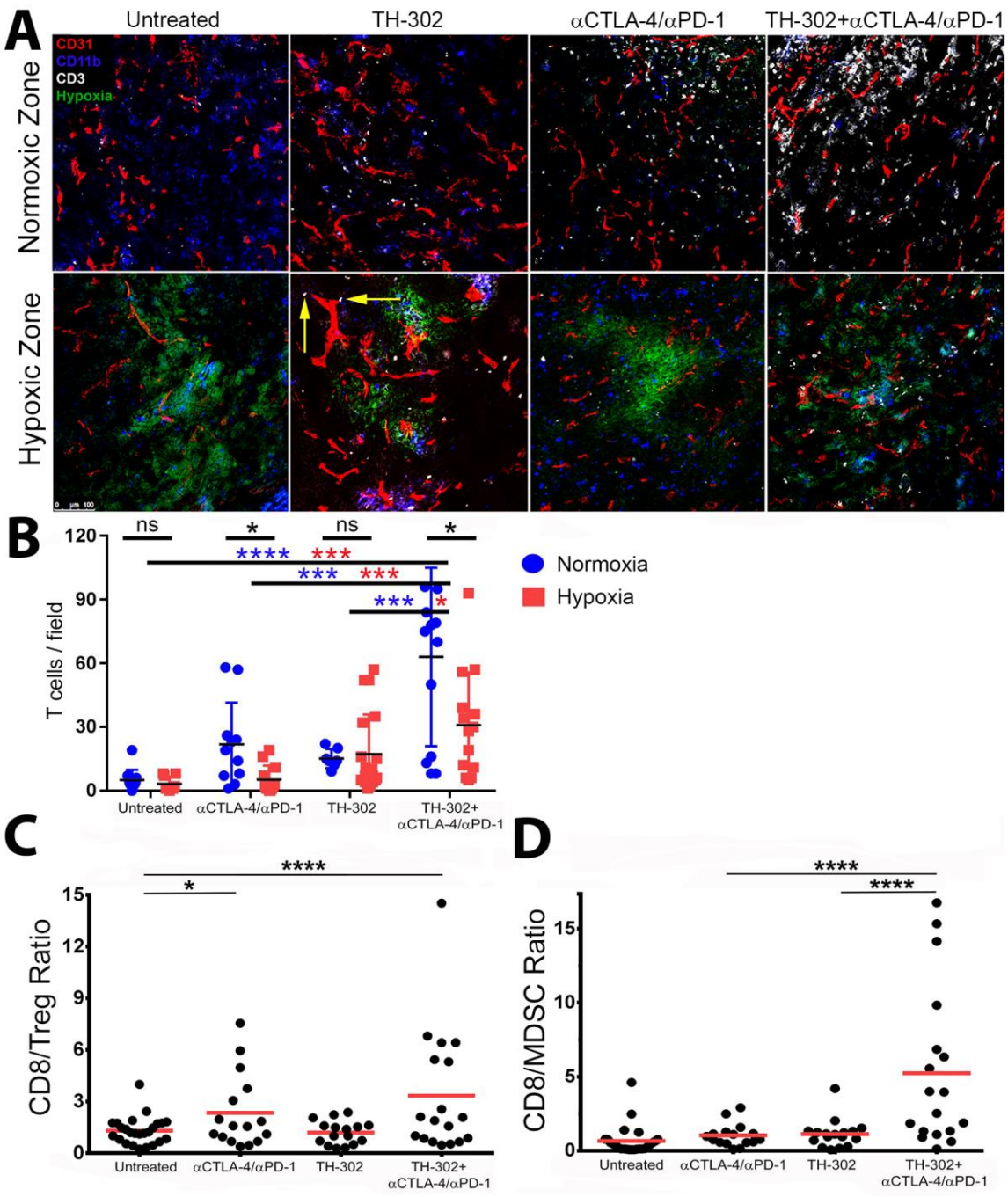

Figure 2. *Hypoxia loss reverses T cell exclusion and suppression in prostate tumors.* (**A**) Mice bearing 14-day pre-implanted TRAMP-C2 tumors were treated with one cycle of TH-302 and/or antibody therapy. Tumors were isolated, OCT mounted, frozen, sectioned, fixed, and stained for pimonidazole(FITC), CD31(Alexa 647), CD11b(Alexa 546), and CD3(V450). (**B**) Quantification of $CD3^+$ T cells from tumors of mice treated in **A**. $CD3^+$ T cells in at least 10 fields per tumor were counted and at least 2 tumors/condition were analyzed. The average $CD3^+$ T cell number per field is shown. (**C**) Mice were implanted with TRAMP-C2 tumors in 30% Matrigel and treated beginning on day 14 for 2 cycles of therapy. One day following therapy, tumor

infiltrating lymphocytes were purified and analyzed by flow cytometry. The intratumoral ratios of $CD3^+CD8^+$ T cells versus $CD3^+CD4^+FoxP3^+$ Treg cells and (**D**) $CD11b^+Gr\text{-}1^+Arginase^+$ MDSC are shown. **C** and **D** are individual mice from 5 independent experiments. Statistical significance between groups was determined by ANOVA. ns = not significant * = P<0.05, ** = P<0.01, *** = P<0.001, **** = P<0.0001.

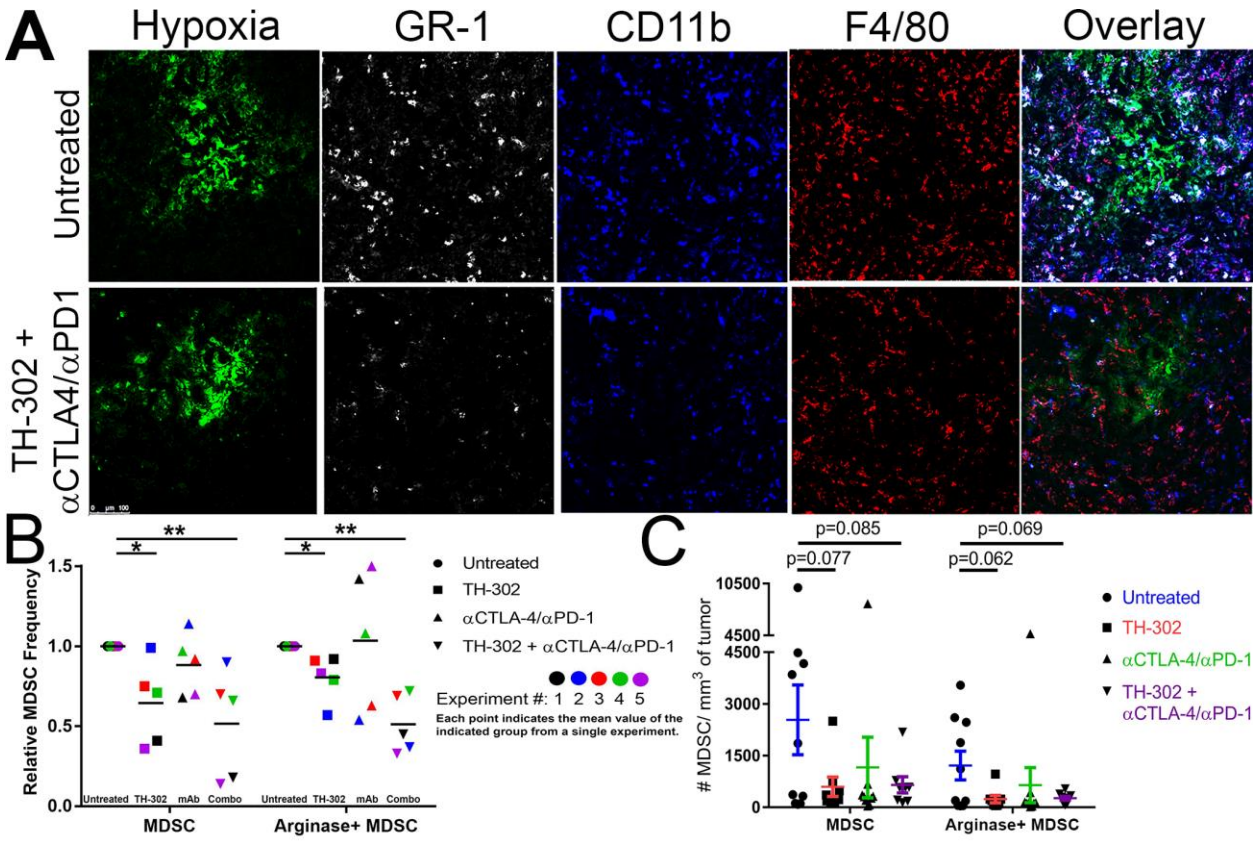

Figure 3. *Hypoxia ablation reduces the frequency and density of MDSC in the tumor microenvironment.* (**A**) 2 week pre-established TRAMP-C2 tumors were treated with TH-302 and antibody for one cycle of therapy and then tumors were isolated, fixed, embedded in OCT, sectioned, and stained for pimonidazole (FITC), Gr-1 (V450), CD11b (Alexa 546) and F4/80 (Alexa 647). (**B**) Mice were implanted with TRAMP-C2 tumors in 30% Matrigel and treated beginning on day 14 for 2 cycles of therapy. The day after conclusion of therapy, tumor infiltrating MDSC were purified and analyzed by flow cytometry. The frequencies of $CD11b^{+}Gr\text{-}1^{+}$ and $CD11b^{+}Gr\text{-}1^{+}Arginase^{+}$ MDSC relative to untreated animals are shown for 5 independent experiments each with 3-10 mice per group. (**C**) The absolute densities of $CD11b^{+}Gr\text{-}1^{+}$ and $CD11b^{+}Gr\text{-}1^{+}Arginase^{+}$ MDSC relative to untreated animals are shown for 2 independent experiments each with 3-10 mice per group. Statistical significance between groups was determined by ANOVA. ns = not significant * = P<0.05, ** = P<0.01, *** = P<0.001, **** = P<0.0001.

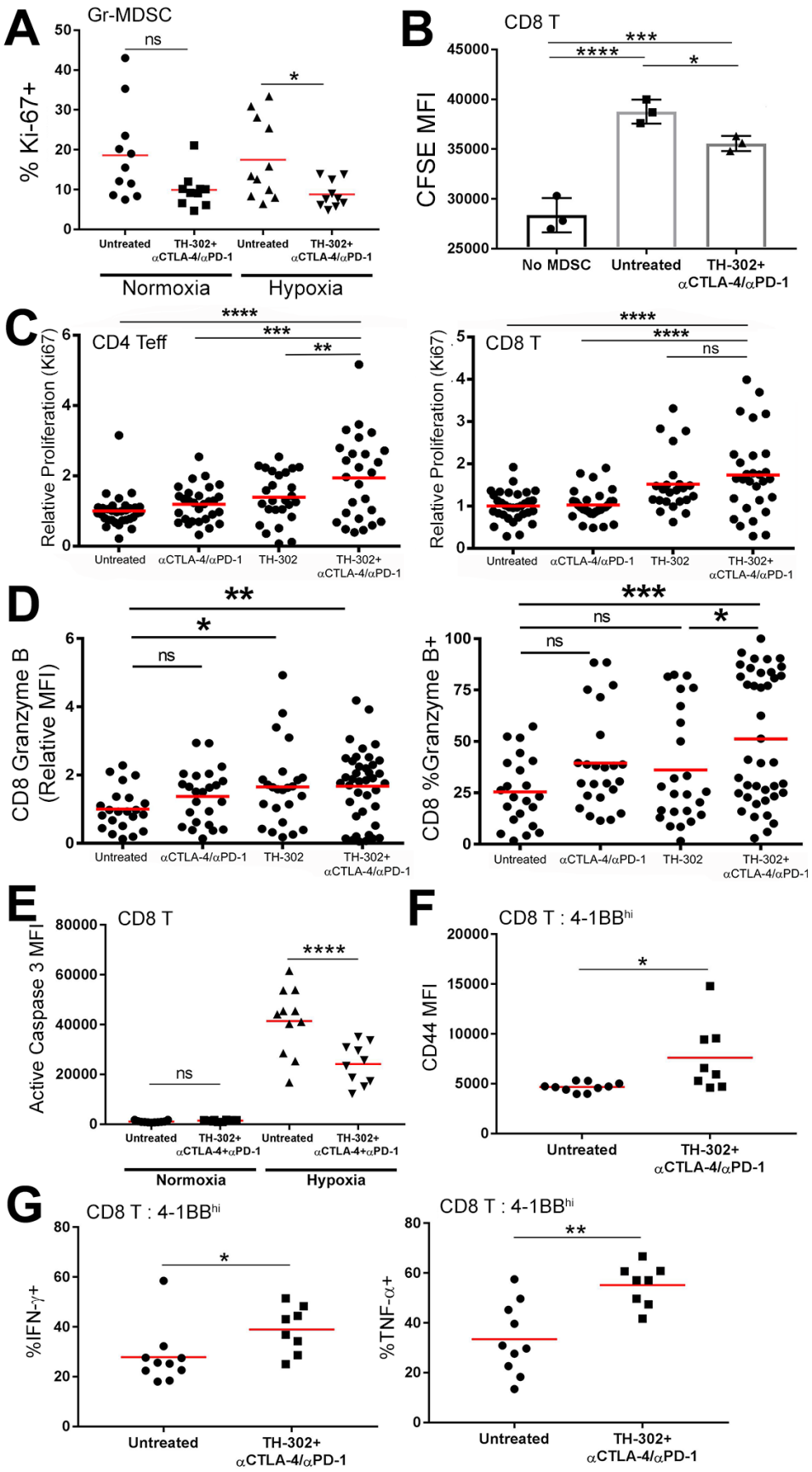
A
Gr-MDSC
% Ki-67+
ns
*
Untreated
TH-302+ αCTLA-4/αPD-1
Untreated
TH-302+ αCTLA-4/αPD-1
Normoxia
Hypoxia
B
CD8 T
CFSE MFI
***
****
*
No MDSC
Untreated
TH-302+ αCTLA-4/αPD-1
C
CD4 Teff
Relative Proliferation (Ki67)
****
***
**
Untreated
αCTLA-4/αPD-1
TH-302
TH-302+ αCTLA-4/αPD-1
CD8 T
Relative Proliferation (Ki67)
****
****
ns
Untreated
αCTLA-4/αPD-1
TH-302
TH-302+ αCTLA-4/αPD-1
D
CD8 Granzyme B (Relative MFI)
**
*
ns
Untreated
αCTLA-4/αPD-1
TH-302
TH-302+ αCTLA-4/αPD-1
CD8 %Granzyme B+
***
ns
*
ns
Untreated
αCTLA-4/αPD-1
TH-302
TH-302+ αCTLA-4/αPD-1
E
CD8 T
Active Caspase 3 MFI
****
ns
Untreated
TH-302+ αCTLA-4+αPD-1
Untreated
TH-302+ αCTLA-4+αPD-1
Normoxia
Hypoxia
F
CD8 T : 4-1BBhi
CD44 MFI
*
Untreated
TH-302+ αCTLA-4/αPD-1
G
CD8 T : 4-1BBhi
%IFN-γ+
*
Untreated
TH-302+ αCTLA-4/αPD-1
CD8 T : 4-1BBhi
%TNF-α+
**
Untreated
TH-302+ αCTLA-4/αPD-1

Figure 4. *Combined hypoxia ablation and checkpoint blockade decreases MDSC suppressive capacity and promotes T cell effector function***.** (**A**) Mice were implanted with TRAMP-C2 tumors in 30% Matrigel and treated beginning on day 21 for 1 cycle. Two days later, mice were injected with pimonidazole and euthanized 6 hours later. Proliferation of tumor infiltrating Gr-MDSC ($CD11b^{+}Ly\text{-}6G^{+}Ly\text{-}6C^{-}$) cells in $pimonidazole^{-}$ (normoxia) and $pimonidazole^{+}$ (hypoxia) regions was assessed by Ki67 staining (6-7m/group, n=1). (**B**) Mice were treated as **A** but for 2 cycles of therapy. Two days later, tumor-infiltrating $CD11b^{+}Gr\text{-}1^{+}$ MDSC were sorted and co-cultured with αCD3/ αCD28 activated T cells for 72 hours. T cell proliferation was assessed by CFSE dilution. Tumors from 14-16 mice with bilateral tumors were pooled for each condition. (**C**) Mice treated as **B** but starting at day 14. The next day, tumor infiltrating lymphocytes were purified and analyzed by flow cytometry for Ki67 (proliferation) expression and (**D**) Granzyme B (cytotoxic potential) expression (n=5). (**E**) Mice were treated as in **A** and apoptosis of tumor-infiltrating $TCR\beta^{+}CD8^{+}$ T cells in $pimonidazole^{-}$ (normoxia) and $pimonidazole^{+}$ (hypoxia) regions was assessed by active Caspase-3 staining (6-7m/group, n=1). (**F**) Mice were treated as in **A**. The next day, tumor-infiltrating $TCR\beta^{+}CD8^{+}$ T cells were isolated and activated for 5 hours using the Leukocyte Activation Cocktail with Golgi Plug (BD Biosciences) and assessed for expression of CD44 and (**G**) IFN-γ and TNF-α in the $4\text{-}1BB^{med/hi}$ subset of CD8 T cells (10m/group, n=1). Statistical significance between groups was determined by Student's t test for **A**, **E-G** and by ANOVA for **B-D**: ns = not significant * = P<0.05, ** = P<0.01, *** = P<0.001, **** = P<0.0001.

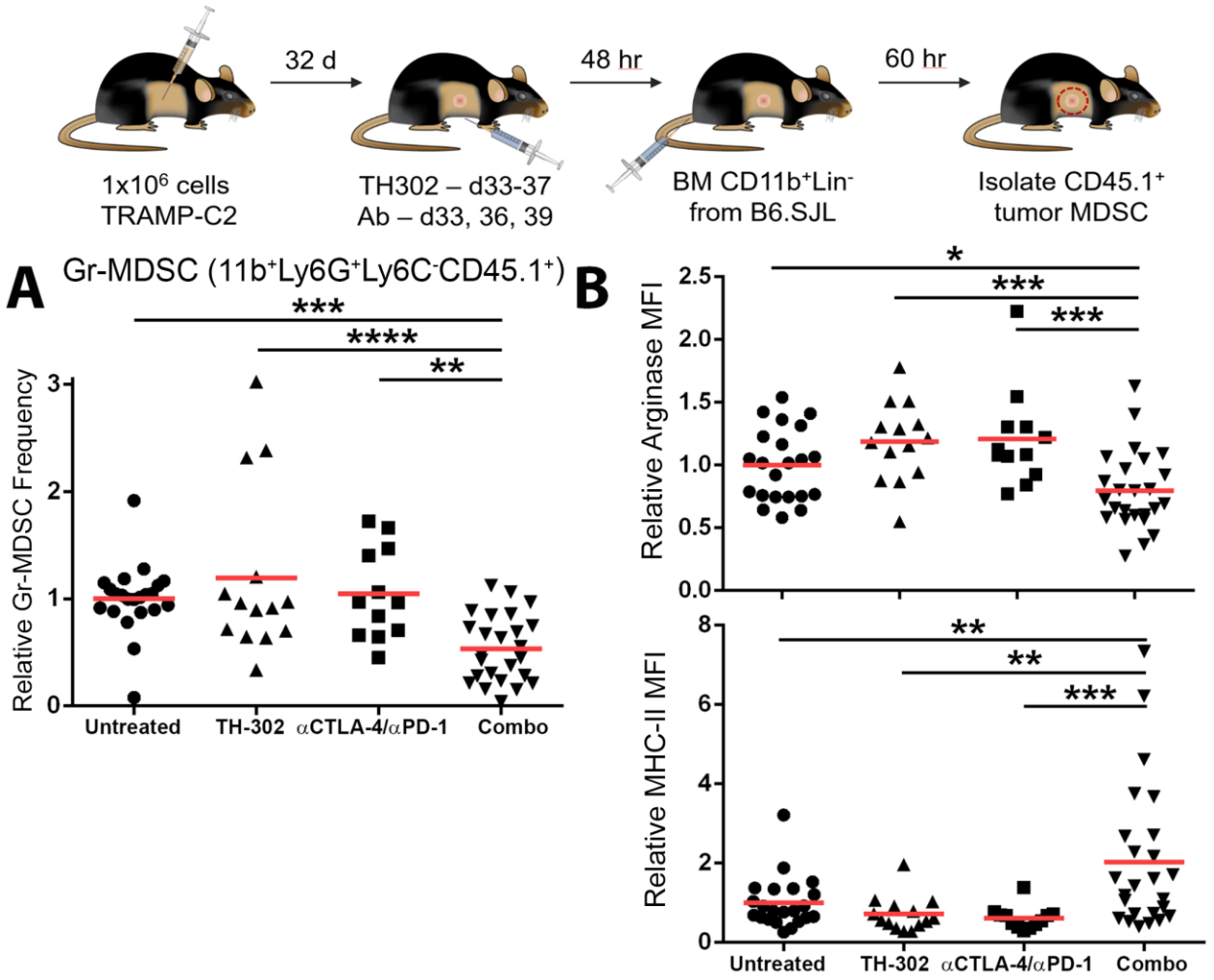

Figure 5. *Hypoxia ablation and checkpoint blockade causes persistent defects in the capacity of prostate tumors to replenish their Gr-MDSC.* (**A**) 32-day pre-established TRAMP-C2 tumors were treated with TH-302 and antibody or left untreated and then immature bone marrow myeloid cells($CD11b^+lin^-$) from B6.SJL ($CD45.1^+$) mice were injected via tail vein. After 60 hours tumor infiltrating myeloid cells were isolated and analyzed by flow cytometry. The frequency of tumor infiltrating $CD45.1^+$ myeloid cells polarized to Gr-MDSC ($CD11b^+Ly6G^+Ly6C^-CD45.1^+$) is shown relative to untreated animals. (**B**) The phenotype of Gr-MDSC ($CD11b^+Ly6G^+Ly6C^-CD45.1^+$) cells is shown for Arginase and MHCII expression (mean fluorescence intensity relative to untreated). 5-10 mice/group, n=2. Statistical significance between groups was determined by ANOVA. ns = not significant * = P<0.05, ** = P<0.01, *** = P<0.001, **** = P<0.0001.

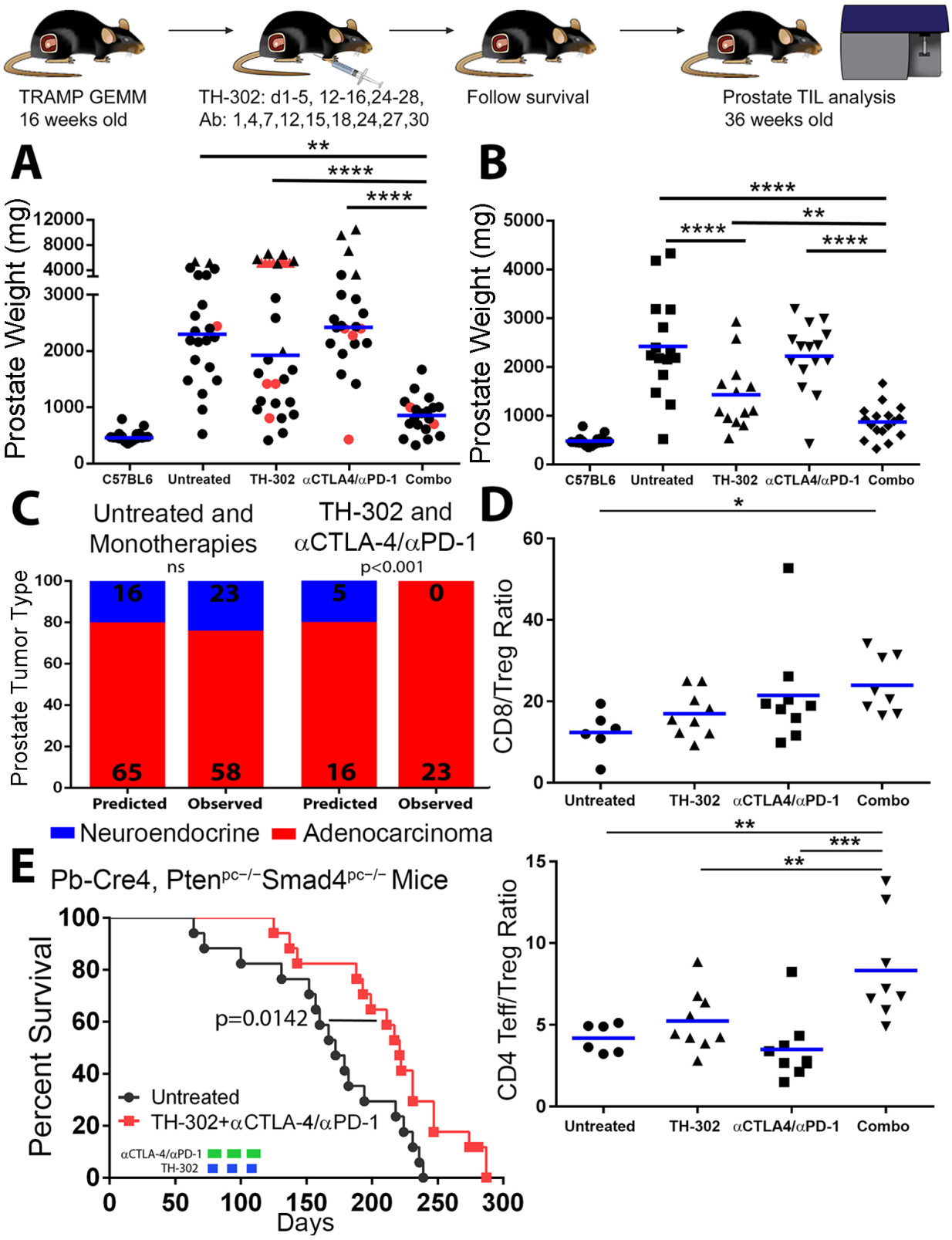
TRAMP GEMM
16 weeks old
TH-302: d1-5, 12-16,24-28,
Ab: 1,4,7,12,15,18,24,27,30
Follow survival
Prostate TIL analysis
36 weeks old
A
Prostate Weight (mg)
C57BL6
Untreated
TH-302
αCTLA4/αPD-1
Combo
B
Prostate Weight (mg)
C57BL6
Untreated
TH-302
αCTLA4/αPD-1
Combo
C
Untreated and Monotherapies
TH-302 and αCTLA-4/αPD-1
ns
p<0.001
Prostate Tumor Type
Predicted
Observed
Predicted
Observed
Neuroendocrine
Adenocarcinoma
D
CD8/Treg Ratio
Untreated
TH-302
αCTLA4/αPD-1
Combo
CD4 Teff/Treg Ratio
Untreated
TH-302
αCTLA4/αPD-1
Combo
E
Pb-Cre4, Ptenpc−/−Smad4pc−/− Mice
Percent Survival
p=0.0142
Untreated
TH-302+αCTLA-4/αPD-1
αCTLA-4/αPD-1
TH-302
Days

Figure 6. *Hypoxia ablation and checkpoint blockade combine to control spontaneous prostate tumors in TRAMP transgenic mice.* TRAMP mice were treated at 16 weeks for 3 cycles with TH-302 and/or antibody and euthanized at 36 weeks and their prostates weighed. (**A**) Mice that died prior to 36 weeks are shown in red, survivors black. Adenocarcinomas are indicated by circles and neuroendocrine carcinomas as triangles. Average weight of early death neuroendocrine tumors (some red triangles) are shown where tumors could not be freshly weighed. (**B**) Only adenocarcinomas from mice that lived to 36 weeks are shown. (**C**) Predicted distribution of adenocarcinomas versus neuroendocrine cancer in these mice based on historical data are shown compared to the observed values for "Untreated + Monotherapy" (sum of no treatment, anti-CTLA-4/anti-PD-1 alone, TH-302 alone) versus "TH-302 + anti-CTLA-4/anti-PD-1". p values calculated using 1-sample proportion test compared to historical 80%:20% adenocarcinoma to neuroendocrine frequency. (**D**) Prostate tissue isolated from 36-week old TRAMP transgenic mice was dispersed into single cell suspension and analyzed by flow cytometry. Ratios of CD8 and CD4 FoxP3^{-} Teff are shown relative to CD4 FoxP3^{+} Treg for all mice pooled from 3 independent experiments. Statistical significance between groups for **A**,**B**,and **D** was determined by ANOVA. ns = not significant * = P<0.05, ** = P<0.01, *** = P<0.001, **** = P<0.0001. (**E**) *Pb-Cre4, Pten*$^{pc-/-}$*Smad4*$^{pc-/-}$ mice were treated as in **A** beginning at 12 weeks of age and followed for survival. Statistical significance was calculated using the log-rank (Mantel-Cox) test.